Spiropyran mechano-activation in model silica-filled elastomer nanocomposites reveals how macroscopic stress in uniaxial tension transfers from filler/filler contacts to highly stretched polymer strands

Yinjun Chen, Artem Kovalenko, Annie Brûlet, Bruno Bresson, Alexandre Lantheaume, Ludovic Olanier, Costantino Creton

Spiropyran mechano-activation in model silica-filled elastomer nanocomposites reveals how macroscopic stress in uniaxial tension transfers from filler/filler contacts to highly stretched polymer strands.

Yinjun Chen[1, 2], Artem Kovalenko*[2], Annie Brûlet[3], Bruno Bresson[2], Alexandre Lanthaume[2], Ludovic Olanier[2], Costantino Creton*[2]

1- State Key Laboratory for Modification of Chemical Fibers and Polymer Materials, College of Materials Science and Engineering, Donghua University, Shanghai 201620, P. R. China

2- Laboratoire Sciences et Ingénierie de la Matière Molle, ESPCI Paris, PSL University, Sorbonne Université, CNRS, F-75005 Paris, France

3 - Laboratoire Léon Brillouin, UMR12 CEA-CNRS, Université Paris-Saclay, CEA-Saclay, F-91191 Gif-sur-Yvette, France

For Table of Contents use only

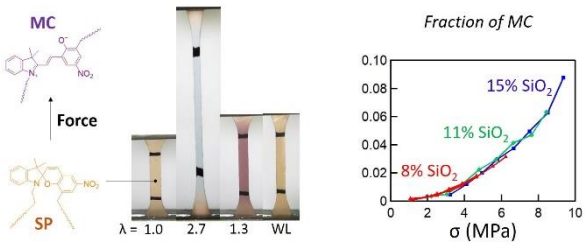

Abstract

Mechanochemistry has proved to be a powerful tool to map the stress distribution and quantify covalent bond scission occurring when model polymer networks, such as elastomers and gels, are deformed and fractured. In the current work, we incorporate a mechanochromic non-scission type mechanophore, spiropyran (SP) in the elastomeric matrix of nanosilica-filled cross-linked poly(ethylacrylate) nanocomposites (PEANC) containing different filler volume fractions and different filler/matrix interfacial properties. The branched fractal-like morphology of the fillers (characterized by X-ray scattering, AFM and SEM) and the mechanical properties of our samples in uniaxial tension are similar to the industrially used elastomer nanocomposites. Under tensile loading, the PEANC samples change their color and the concentration of mechanophores activated into merocyanine can be quantified from absorption spectra. Results show that, in uniaxial tension SP activation is governed by the peak nominal stress applied to the sample resulting in a master curve of activated SP fraction as a function of stress, independent of the filler volume fraction and interfacial coupling. Upon several loading cycles to the same stretch level, the concentration of activated SP decreases moderately, especially at high stretch. The activation of mechanochromic molecules support the hypothesis of a two-stages toughening mechanism of nanocomposites. At low strain the load is mostly carried by fractal-like aggregates of silica filler, while at high strain the load is transferred from the physical network of filler particles to the highly stretched polymer chains surrounding the aggregates. This scenario supports the dominant role played by the limited extensibility of polymer chains in the nanocomposite stiffening. The labeling of polymer networks with mechanosensitive molecules provides here a clear visual pathway to the mechanisms responsible for stiffening, and ultimately toughening, of nanocomposites.

Introduction

An important application of mechanochemistry has proved to be the reporting of covalent bond scission or of molecular forces acting on covalent bonds in soft polymer-based networks. Force-sensitive moieties, namely, mechanophores, can be incorporated into the polymer backbones or as crosslinkers. If the material is deformed, the mechanophores experience a mechanical force and can in return undergo a chemical reaction that can change the optical properties of the material.[1] While the activation of mechanophores by force can lead to various mechanoresponsive features[2], including mechanocatalysis, mechanochromism, mechanoluminescence, mechanofluorescence, release of small molecules, etc, we will focus here on non-scissile mechanophores that change their absorption properties in the visible range. This change in absorption is ideal for real time measurements.

The intensity of the mechano-optical response is determined by the activated fraction of mechanophores, which depends on the magnitude of the stress or strain. Consequently, a space resolved quantification of the optical response enables mapping of the stress[3–5] and/or damage[6] distribution in soft polymer materials. However, simple elastomeric and hydrogel networks are usually fragile and break by crack propagation at a low value of applied stretch resulting in very little mechanophore activation in the bulk of the sample. The recent investigation of broken samples containing scissile fluorophores showed a strong localization of the activation near the fracture surface for these simple networks[7]. While the activation may also be analyzed in compression experiments, a geometry where samples typically can withstand much higher degrees of deformation without breaking[8], it is more interesting to understand in which conditions mechanophores can be activated in the bulk in uniaxial tension. The progressive level of activation in the bulk as the sample is strained, may bring

evidence for a toughening mechanism since bond scission in the bulk *is* an energy dissipation mechanism that can contribute to delaying the propagation of a macroscopic crack.

The mechanical reinforcement (increase in fracture strength and toughness) of elastomer networks can be obtained by the incorporation of supramolecular interactions[9], sacrificial networks[6] or nano-fillers[10]. Upon loading, the supramolecular interactions and sacrificial networks dissipate energy via reversibly breaking weak bonds or irreversibly breaking covalent bonds. This bond scission must occur in the bulk of the elastomer or at least up to a certain distance from the crack plane to be effective as a toughening mechanism.

The incorporation of scissile and non-scissile mechanophores in interpenetrated multiple network elastomers made it possible to prove the underlying toughening mechanisms of these materials at the molecular level[6,7,11,12]. However, these tough networks are still "exotic" and not used for industrial applications where the most relevant and cheap method of toughening elastomers remains the introduction of nanofillers, usually silica and/or carbon black nanoparticles. The mechanical properties of such filled elastomers display some characteristic features, such as for example, an irreversible softening (Mullins effect[13]) and sometimes nanocavitation[14–16] in large strain and a strain-dependent modulus in small strain (Payne effect[17,18]).

Despite the technological relevance of elastomer nanocomposites, the reinforcement mechanism by nanofillers is still not completely understood, especially at high strains when the polymer chains are highly stretched which may cause irreversible network damage. The incorporation of mechanophores in nanocomposites offers a great opportunity to tackle this problem. For example, Clough et al.[19] incorporated dioxetane mechanophore into silica-filled poly(dimethylsiloxane) elastomers and demonstrated that the network bond scission

contributed to the Mullins effect by monitoring the mechanoluminescence in cyclic tensile tests. Kim et al.[10] synthesized different spiropyran probes which could be either grafted on the surface of silica nanoparticles or polymerized in the bulk of the poly(methylacrylate) matrix. The samples with mechanophore localized on the silica surface demonstrated much stronger activation compared to those with the mechanophores distributed in the matrix. This effect was attributed to the "interfacial force focusing", i.e. high stress concentration in the polymer confined between filler particles. However, it is still challenging to fabricate mechanophore-tagged nanocomposites with a relatively simple composition and mechanical properties comparable to those of the industrial ones. Quantitative analysis of the mechano-activation in such model nanocomposites will shine light on the molecular origins of the stress-strain response at high strain. In particular, the incorporation of non-scissile mechanophores, such as spiropyran cross-linkers, may sense the stress partitioning between the filler network and the matrix. This partition most likely evolves under stretch due to the non-affine deformation of the filler network, as confirmed recently by transmission electron microscopy[20] and conductivity measurements[21].

Herein, poly(ethyl acrylate) elastomers reinforced with fractal silica nanoparticles were labeled with a dilute amount of spiropyran mechanophore molecular probe which activates when the polymer chains are highly stretched. The preparation of the nanocomposite was carried out in mild conditions to avoid thermal degradation of the SP. By quantitatively analyzing the spiropyran color change after cycles of tensile loading using a previously reported calibration method[22], we obtain the activation of the mechanophore, and hence the concentration of highly stretched polymer strands, as a function of the stress and strain. We applied this method to nanocomposites containing different silica volume fraction and different amount of filler/matrix interfacial coupling agents.

2. Materials and Methods

2.1. Chemicals

Ethyl acrylate monomer and 1.4-butanediol diacrylate cross-linker were purchased from Sigma Aldrich and purified by passing through an alumina column. Thixosil T365 silica nanoparticles with a specific surface area of 150 m^2/g were donated by Solvay. Lauroyl peroxide (Sigma Aldrich) was used as thermal initiator. We used two surface-coupling agents: the non-covalent chloro(dimethyl)octylsilane (DMOS) and the covalent chloro(dimethyl)vinylsilane (DMVS), both obtained from Sigma Aldrich. Spiropyran (SP) diacrylate cross-linker was synthesized following a previously reported protocol[11].

2.2. Nanocomposite fabrication

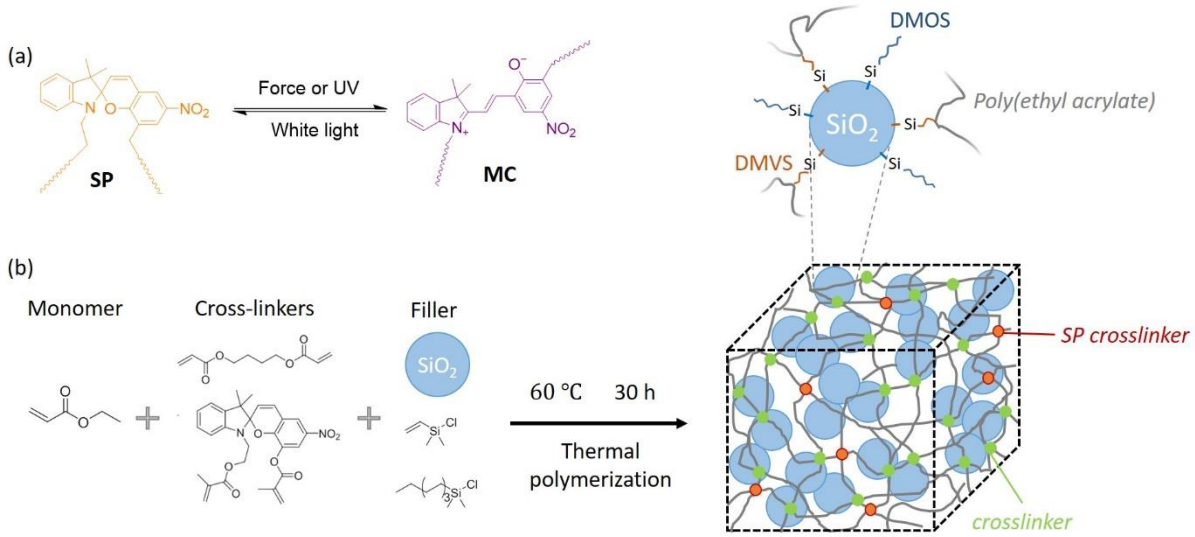

Figure 1 – (a) Spiropyran (SP) is activated into merocyanine (MC) under the stimulation of extra force or UV light and the reverse reaction occurs by irradiating with a strong white light source; (b) The scheme of the synthesis of nanocomposites with SP.

Table 1 shows the typical amounts of reagents used to synthesize the nanocomposites which is schematized on the Figure 1. To avoid contamination with oxygen, the mixing and polymerization were carried out in a glovebox. Silica nanoparticles were mixed with a pre-polymer solution consisting of ethyl acrylate monomer (10 g), 1,4-butanediol diacrylate (BDA) (0.1 g), spiropyran diacrylate (0.05 g) crosslinkers, and lauroyl peroxide initiator (40 mg). For a covalent coupling between silica particles and polymer matrix, a mixture composed of chloro(dimethyl)octylsilane (DMOS) and chloro(dimethyl)vinylsilane (DMVS) was added to the pre-polymer solutions. The use of the monodentate grafting ligands avoids the problem of possible formation of a poly(siloxane) network via hydrolysis. The mixture of silica particles and the pre-polymer solution was shaked in a closed bottle by an alternating action of a vibrational mixer and ultrasound to obtain a homogeneous liquid paste. Due to the high reactivity of chlorosilanes, the grafting and hydrophobization of nanoparticles was very rapid (a few minutes) as seen from the evolution of the dispersion state of silica in the acrylate monomers during homogenization. The homogeneous paste was then poured into a glass mold with a 1 mm silicone rubber spacer and sealed. The mold was in turn sealed into a plastic bag using a vacuum sealer. Thermal polymerization was carried out at 60°C for 30 hours in a water bath. The resulting composite films were washed with a mixture of ethanol and acetone (1:1). To avoid the formation of cracks during drying, polymer films were dried at normal pressure and temperature for 24 h, then dried in vacuum for 48 h resulting in composite films. To synthesize different composite polymer materials, the weight of silica particles and the ratio of DMOS/DMVS was varied as shown in Table 1. Additionally, an unfilled poly(ethyl acrylate) network was synthesized by thermal polymerization as a reference sample.

Hereafter, for the simplification of the description, the composites are referred to as NPxVSy, where NP, VS, x and y are used for nanoparticles (when present), DMVS, the weight of silica particles and the presence or absence of DMVS, respectively. EA represents the blank samples.

Table 1 – Composition of the nanocomposite samples

Polymers	Silica	EA	SP	BDA	DMOS		DMVS	
	g	g	g	g	% of silane	g	% of silane	g
EA	0	10	0.05	0.1	0	0	0	0
NP1VS1	1	10	0.05	0.1	88	.088	12	0.013
NP2VS1	2	10	0.05	0.1	88	0.175	12	0.025
NP3VS1	3	10	0.05	0.1	88	0.252	12	0.038
NP4VS1	4	10	0.05	0.1	88	0.350	12	0.050
NP4VS0	4	10	0.05	0.1	100	0.400	0	0

2.3. Composite characterization

The final fraction of silica nanoparticles in the elastomer was determined by thermogravimetric analysis (TGA) using a SDT600 device (TA Instruments) in a synthetic air atmosphere. The heating cycle was composed of a ramp at 5°C/min from room temperature to 350°C, a plateau of 15 min at 350°C and a ramp at 5°C/min to 700°C. The TGA curves (Figure SI.1) confirmed that the final mass fraction of silica is similar to the expected one. The slight differences may be due to the monomer evaporation during the transfer from the mixing vial

to the mold. Assuming the density of the polymer matrix equal to 1.12 g/cm^3 and that of SiO_2 equal to 2.2 g/cm^3, the volume fractions of silica in the nanocomposites were calculated and the results are shown in Table 2. The maximum volume fraction was about 15 %, which is in the typical range for the most common nanocomposites.

We used small angle X-ray scattering to probe the filler structure. SAXS experiments were carried out on the Xeuss 2.0 apparatus (Xenocs) of LLB installed in the SWAXS-Lab (Saclay, France). The instrument uses a Genix 2D Cu source (wavelength of 1.54189 Å) and a Pilatus3 1M detector (Dectris).

Two configurations were used to cover a broad q range from 0.028 to 4.5 nm^{-1}: first, a sample to detector distance set to 1.19 m with a collimated beam size of 0.4 × 0.4 mm^2, second, a sample to detector distance set to 2.49 m with a collimated beam size of 0.25 × 0.25 mm^2. The measurements were carried out for 10 minutes and 60 minutes respectively to get good statistics in the two configurations. The incident beam flux can be directly measured on the detector. The scattering from the empty beam and electronic background (dark) were subtracted using standard protocols[23]. Scattering intensities, normalized by the sample's thickness, are given in absolute units, cm^{-1}.

Atomic force microscopy (AFM) characterization was performed on freeze-fractured samples using a Bruker ICON microscope in the tapping mode. In addition, some selected fractured surfaces were coated with a 20 nm gold layer and their surface was observed with a Quattro scanning electron microscope (FEI) in secondary electrons mode.

2.3. Mechanical characterization

Mechanical testing was carried out on an Instron 5565 universal testing machine in uniaxial extension geometry using rectangular samples with a width of 5 mm and thickness of about 1 mm. All the data are recorded with an initial stretch rate $d\lambda/dt = 0.05\ s^{-1}$. The Young's modulus E was determined from the linear fit of the curves up to a strain of 1%. For cyclic loading, the tests were performed between zero stress state and a peak stretch value λ_{max}. The details for determination of the fracture toughness Γ using notched samples are given in the Supporting information (Figure SI.2).

2.4. Mechanophore activation detection

To detect the spiropyran mechano-activation, we used an optical fiber Flame UV-vis spectrometer (Ocean Optics) with a low-intensity tungsten halogen lamp illumination in the visible range. This illumination did not produce any change of the sample color for at least one hour. The spot size of the illumination was about 3 mm in diameter. The intensity of the transmitted light *I* was determined after each loading cycle in the Instron machine using a home-made holder for the optical fibers. The absorbance was calculated as $A = -\log_{10}(I/I_0)$, where I_0 is the transmitted intensity after the inactivation of the spiropyran by irradiation of the sample with a strong white light for about 5 min. To account for the variations between different samples, the absorbance was normalized by the sample thickness d_{sample} and the total mechanophore concentration in the sample C_{SP}^{sample}:

$$A_{norm} = \frac{A}{C_{SP}^{sample} d_{sample}} \qquad (1)$$

The values of A_{norm} were obtained for the visible wavelength range from 400 nm to 800 nm.

Next, to estimate the fraction of the activated mechanophore probes with respect to the total SP which may be activated, we acquired the absorbance spectrum of the samples after

illumination with UV light for 2 minutes, a level of illumination that activates all SP into its MC form. The fraction of activated molecules was estimated by:

$$f_{activ} = \frac{C_{MC}}{C_{MC} + C_{SP}} = \frac{A_{norm}(580\ nm)}{A^{UV}_{norm}(580\ nm)} \quad (2)$$

where A_{norm} (580 nm) and A^{UV}_{norm} (580 nm) are the values of the normalized absorbance at the wavelength 580 nm of the sample before and after UV activation. Note that because of the strong absorption, the A^{UV}_{norm} (580 nm) value was obtained indirectly using a reference sample as described in the Supporting information (see Figure SI.3).

3. Results

3.1. Structural characterization of the obtained nanocomposites

The quality of the dispersion of nanoparticles in the composite films was characterized by SAXS, AFM and SEM measurements. AFM images (Figure 2a and SI.4) show silica aggregates with a branched fractal-like structure, typical of the industrial and simplified industrial nanocomposites[24]. The primary nanoparticles with an average radius R_p ≈ 10-15 nm form aggregates and chain-like structures with typical radii of a few nanoparticles. These primary aggregates exist in bare silica powder because the nucleation and growth of precipitated silica occurs simultaneously. The aggregates form agglomerates with very different sizes and shapes ranging from a few hundreds of nanometers (see the large-scale AFM images on Figure SI.4) to tens of microns (see the SEM images Figure SI.5). The SAXS curves have very similar shapes for all the samples in the accessible range of q-vectors. Normalized by the corresponding silica volume fraction listed in Table 2, the curves superimpose very well (Figure 2b, see also the SI.5 for other representations). Only some small differences are observed at very low q (below 0.006Å^{-1}) with a larger upturn towards larger intensity for the composites with silica volume

fraction of about 14.5%. The absence of a plateau at lower q-vectors down to 0.003 $Å^{-1}$, corresponding to scattering fluctuations ~ 100 nm in size, means that there are no characteristic aggregates of this size. In agreement with the literature[25], we may attribute the power law $q^{-2.1}$ at low q to the diffusion from particle aggregates with a fractal dimension of 2.1. The power law $q^{-3.9}$ observed at higher q corresponds to the Porod-like scattering from the particle/polymer interface. The investigation of characteristic inter-aggregate distances at larger scales was limited by the scattering angle range. The change of slope of the SAXS curves at q_p ~ 0.02 $Å^{-1}$ corresponds to the measured primary particle radius $R_p = \pi/q$ = 15.5 nm, in agreement with the AFM images. Interestingly, the samples NP4VS1 and NP4VS0 show similar morphologies in the SEM (Figure SI.5) and similar SAXS profiles (Figure SI.6) despite the difference in coupling agent. We explain this by the presence of an initially aggregated fractal-like structure[25] in the precipitated silica which is partially preserved during the dispersion in the liquid monomer used to synthesize the matrix.

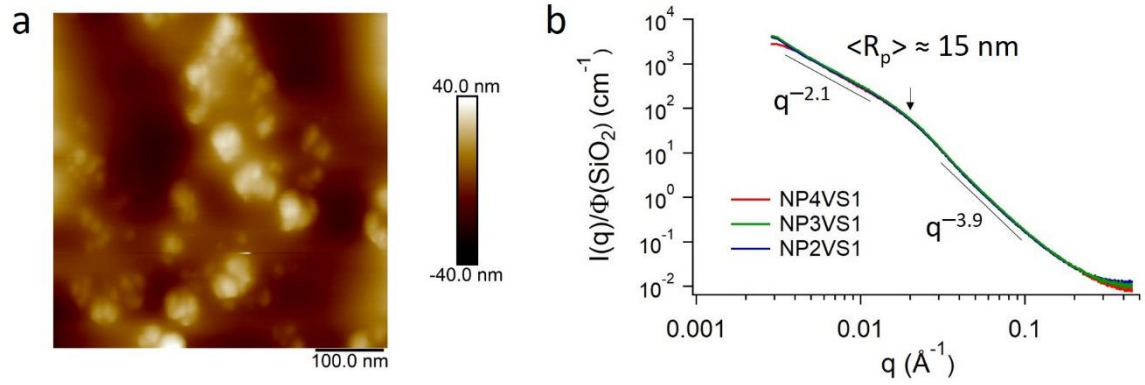

Figure 2 – (a) Atomic force microscopy image of the NP3VS1 sample; (b) small angle X-ray scattering curves obtained from the nanocomposites normalized by the silica volume fraction.

3.2. Mechanical reinforcement

Nanocomposites with varying fractions of silica nanoparticles were tested in tensile loading. Stress-strain curves in Figure 3 illustrate the reinforcement of the poly(ethyl acrylate) matrix by silica nanoparticles for volume fractions of nanoparticles in the range of 0 to 14.5%. Young's moduli and stresses at break are summarized in Table 2 and both significantly increase with volume fraction of silica nanoparticles. Pure poly(ethyl acrylate) network (0% of silica particles) shows a slightly non-linear behavior (Figure 3a) and breaks at a nominal stress of about 0.7 MPa. Adding 4.2% of silica in poly(ethyl acrylate) networks has a little effect on the Young's modulus but significantly increases the maximum extensibility, and the nanocomposite displays the beginning of a strain-hardening behavior. Increasing further Φ_{SiO2} to 8% and 11.4% , increases the modulus and stress at break significantly. For the nanocomposite with 14.5% of silica (NP4VS1), the stress-stretch curve shows a pronounced non-linear behavior at low stretch and no evidence of strain-hardening at high stretch. Due to the covalent links between polymer matrix and silica particles, NP2VS1, NP3VS1 and NP4VS1 samples show a stiffening and toughening relative to the unfilled elastomer that is comparable to what is observed in industrial or "simplified" industrial nanocomposites[15,26,27].

Table 2. The composition of varying polymer composite and their mechanical properties.

Polymers	Silica weight percent (%)	Silica volume fraction (%)	Young's modulus E (MPa)	Stress at break (MPa)
EA	0	0	1.0±0.02	0.7
NP1VS1	9.5	4.2	1.8±0.1	2.1
NP2VS1	18	8.0	3.4±0.2	8
NP3VS1	22	11.4	9.1±0.4	7.3
NP4VS1	28	14.5	30.5±0.7	11.5
NP4VS0	28.5	14.7	16.8±0.3	6.0

Figure 3b shows the Young's modulus E and the fracture toughness Γ of the nanocomposites as a function of the silica volume fraction. The strong increase in Young's modulus (almost 14 times for 14.5% of silica) is characteristic of the reinforcement of elastomers by fractal aggregates, which may percolate even at low volume fractions[28]. This result is in agreement with the observed AFM images. In addition, introducing covalent links between the polymer matrix and the filler surface via DMVS (the sample NP4VS1 with respect to the NP4VS0) has a similar effect as an increase in cross-linking density and is also contributing to the modulus (see values of E and Γ in Table 2). The introduction of fillers increases Γ from 2 to 11 kJ/m^2, reflecting the fact that the increase in modulus is not accompanied by a decrease in maximum extension.

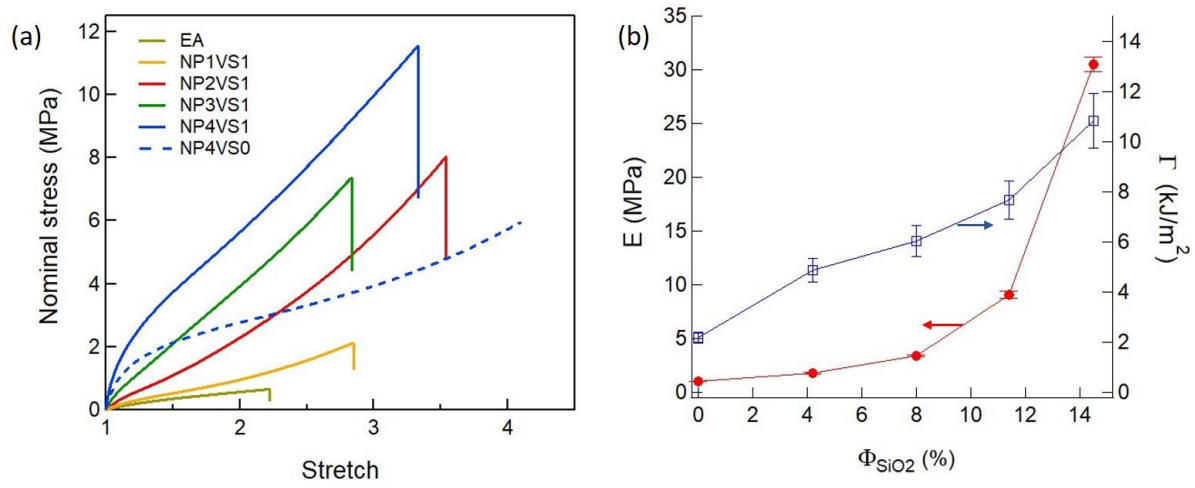

Figure 3 – Mechanical properties of the obtained poly(ethylacrylate) nanocomposites at different silica volume fractions: (a) the stress-stretch curves of unnotched samples in simple extension; (b) the Young's modulus E (red full circles) and fracture toughness Γ (blue open squares) as a function of the filler volume fraction.

3.2. Force-triggered molecular activation

After confirming that the reinforcement of mechanical properties was characteristic of what can be observed in conventional filled elastomers[15,26,27], the mechanical activation of spiropyran was studied as a function of stretch and stretch history. Unlike the unfilled polymer networks, the nanocomposites without spiropyran became markedly white during tensile test, as shown in Figure 4a and Figure SI.7a. The most probable cause of whitening may be attributed to reversible cavitation inside the samples under stress[15,16]. We should note that multiple scattering of the silica aggregates may also influence the transparency of the nanocomposites[29]. Such strong whitening would make it difficult to detect the changes in light absorption caused by SP activation.

However, the white color disappears almost completely upon unloading or after failure of the samples by crack propagation, and it is thus in principle possible to analyze quantitatively the

level of activation of SP in the unloaded state. Yet, in-situ absorbance measurements performed with unlabeled samples (without spiropyran) during a step-cycle tensile loading test (Figure SI.6 b) showed that the transparency was modified at each cycle. Therefore, the image color analysis methodology used in our previous work of mechano-activation determination[3,22] may be incorrect in the case of nanocomposites.

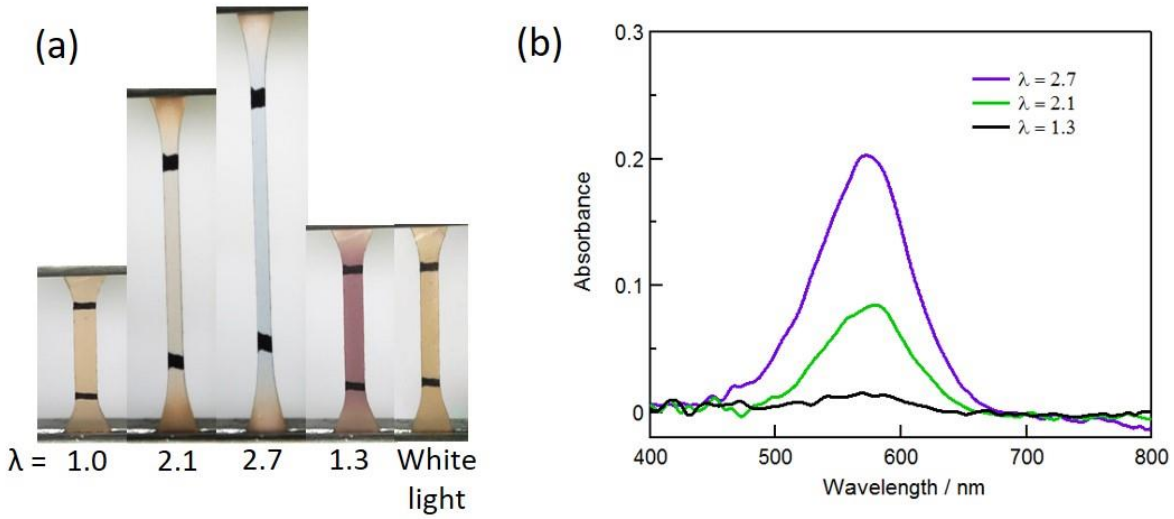

Figure 4 – (a) Photographs of the NP4VS1 sample labeled with SP during one stretching to λ = 2.7 and unloading to zero stress (λ = 1.3); the color during loading is blue and the color upon unloading is purple. We use the purple color to quantify the activation similarly to the ref[22]. The merocyanine is then inactivated by illuminating with a strong white light; (b) the absorbance spectra of spiropyran after cyclic loading to different stretch obtained after removal of the background (the sample illuminated with a strong white light).

To circumvent this problem, we proposed a novel approach to quantify mechanical activation of SP in nanocomposites by measuring the transmittance spectrum of nanocomposite in the unloaded state. Consequently, step cyclic tensile tests were conducted and the transmission spectra of mechano-activated samples were recorded at the end of each cycle (Figure 4a). Subsequently, the sample was irradiated with a strong white light accelerating the

transformation of merocyanine back into SP. The absorption spectrum after illumination was used as a background for each cycle of loading, which enabled to correct the small changes in opacity of the sample in the unloaded state after each cycle. The resulting activation spectra are shown on Figure 4b. The peak centered at 580 nm corresponds to the absorption of MC molecules and its intensity increases with maximum applied stretch λ_{max}. As explained in the experimental section, the value of absorbance at 580 nm was used to quantify the fraction of activated mechanophore f_{activ} in different composites using equation 2.

3.3. Effect of the silica fraction and interfacial coupling

The activation was not detectable for the samples with no silica and 4% of silica because the failure occurred before any measurable level of color change. Figure 5 shows the quantified data of spiropyran activation in three nanocomposites with different silica volume fraction ranging from 8% (NP2VS1) to 14.5% (NP4VS1). Three nanocomposites presented similar step-cycle loading curves (Figure 5a). Each cycle is composed of loading from a zero-load state to a maximum stretch value λ_{max} and unloading to a new zero-load state. The residual stretch values increase with λ_{max} and stay below 1.3. In all cases, the unloading curve lies significantly lower than the loading curve due to the Mullin's effect and viscoelastic hysteresis. Each loading curve of the $(N+1)^{th}$ cycle follows approximately the unloading curve of the N^{th} cycle until its max stretch value $\lambda^{(N)}_{max}$. In the next segment between $\lambda^{(N)}_{max}$ and $\lambda^{(N+1)}_{max}$, the loading follows the path of the first loading of a pristine nanocomposite. The mechanical behavior of nanocomposites is consistent with what is reported in the literature of filled elastomers[13,19,21,30,31].

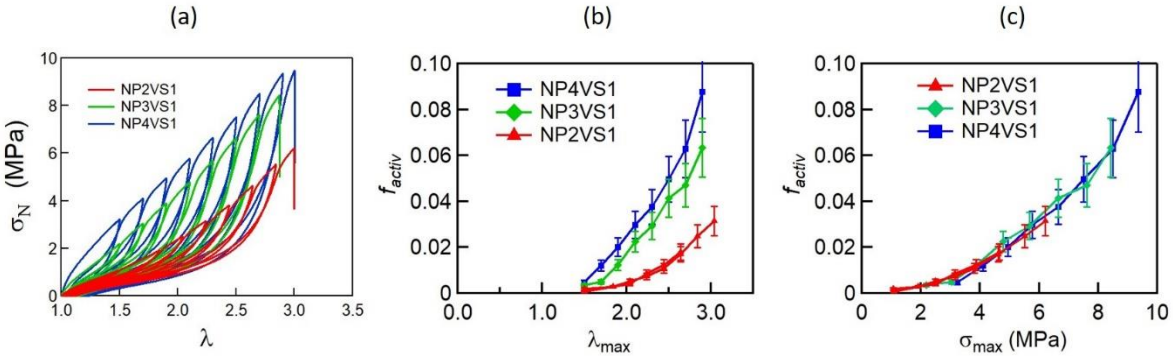

Figure 5 – Mechanophore activation in the cyclic loading of nanocomposites with various volume fraction of silica particles: (a) the stress-stretch curves; (b) the mechanophore activation as a function of λ_{peak} ; (c) the mechanophore activation as a function of the peak stress. The error bars represent the estimated uncertainty related to the absorption analysis.

The fraction of activated mechanophore f_{activ} (denoted as *activation* in the following text) in unloaded samples was measured at the end of each cyclic unloading at a value of $\lambda_{max}(N)$ and $\sigma_{max}(N)$. Figure 5b and c show the activation in nanocomposites after unloading at 580 nm as a function of λ_{max} (the maximum value of stretch in the cycle) and σ_{max} (the maximum value of the stress in the cycle), respectively. In both cases, f_{activ} increases with the maximum loading during the cycle. The non-linear shape of the curves presenting a threshold activation value of around 2 MPa is similar to that observed in unfilled polymer networks at low strain rates[3,8]. For the same value of λ_{max}, the activation is stronger for nanocomposites with a higher filler loading. Interestingly, when the elastomers are loaded to the same σ_{max}, the activation values upon unloading are very similar between the three nanocomposites: the three curves shown in Figure 5c seem to follow a master curve. This result is rather surprising because the stress distribution in nanocomposites is generally considered as very heterogeneous and dependent on the filler fraction and type of aggregation[10,20,28]. However, this surprising result well agree with the similar structures deduced from the SAXS curves of the different nanocomposites:

curves perfectly superimpose down to 0.006Å^{-1} (i.e. for structures up to 100nm) while the filler fractions are different.

3.4. Effect of interfacial coupling on activation

After the measurement of SP activation in nanocomposites with varying volume fractions of silica particles, we now examine the influence of the level of covalent coupling between nanoparticles and polymer matrix. Nanocomposites with a similar volume fraction of silica (ϕ = 14,5%) but different concentrations of the covalent coupling agent (the DMVS) were submitted to step-cycle loaded tests. We note that when the concentration of DMVS increased to twice that of NP4VS1, NP4VS2 (not shown here) the sample showed a strong irreversible cavitation upon stretching to $\lambda \approx 1.5$, resulting in the impossibility to quantify the mechano-activation. Hence, NP4VS1 is compared with NP4VS0 sample (without any DMVS). Stress-strain curves of NP4VS1 and NP4VS0 are shown in Figure 6. We observe that the covalent binding of the matrix to the silica impacts significantly the properties at intermediate and high stretch. NP4VS0 has an "elasto-plastic" behavior with a higher residual stretch (about 1.7) and a sort of plateau at about 2 MPa. This can be explained[15] by the possible slippage and detachment between polymer matrix and the filler, which is hindered by the covalent linkers in the NP4VS1 sample. The elastoplastic behavior induces stronger stress relaxation and creep in the NP4VS0 samples which leads to higher dispersion of the activation values with respect to NP4VS1. As consequence, three different pieces of NP4VS0 presented great differences in activation values for the same λ_{max} in comparison with NP4VS1 as shown in Figure 6b. Interestingly, the activation values as a function of peak stress of both NP4VS1 and NP4VS0

samples appeared to fall on a master curve. These results again validated the strong correlation between nominal stress and SP mechano-activation.

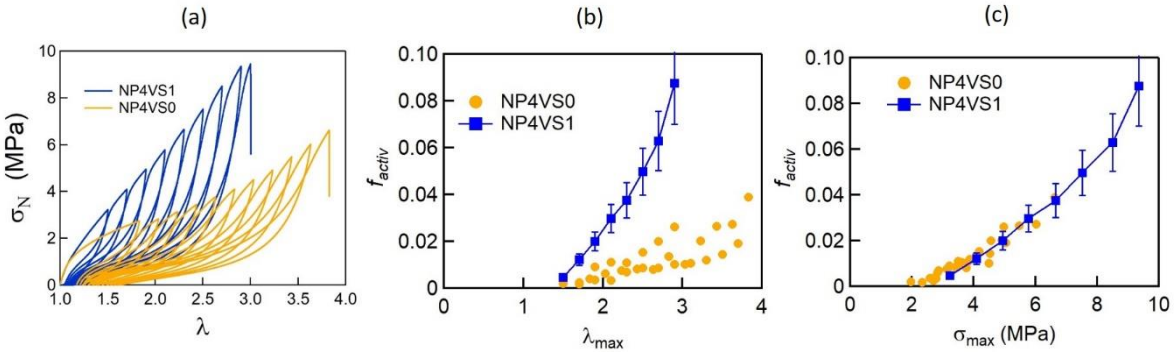

Figure 6 – Mechanophore activation in the cyclic loading of nanocomposites with similar volume fraction of silica particles (14,5%) with covalent (sample NP4VS1) or non-covalent (sample NP4VS0) surface coupling between fillers and the matrix: (a) the stress-strain curves; (b) the mechanophore activation as a function of λ_{peak} ; (c) the mechanophore activation as a function of the peak stress. No error bars are given for the NP4VS0 sample because of the high dispersion of the values, which are caused by elastoplastic behavior.

3.5. Mullins effect

Once validated as a stress sensor, the SP molecular probe activation can also be used to quantify the level of irreversible damage in nanocomposites (Mullins effect) during stretch. Figure 7a shows a selection of stress-strain curves of step-cycle tensile tests. In the cyclic tensile tests, three loading-unloading cycles were carried out for each value of λ_{max}. In the second and third cycles of loading to the same λ_{max} = 1.5, σ_{max} is slightly lower due to the damage in nanocomposite networks in the previous cycle. When loaded to a stretch value higher than λ_{max} (and equal to 1.7 in this figure), the curve follows the mechanical curve of a virgin sample above the previously achieved λ_{max} . We compared the activation curve plotted

as a function of maximum stress in each cycle shown on Figure 7b. The values in the first cycle are about 10-20% higher than those for the second and third cycles. This supports the idea of damage of polymer chains in the first cyclic loading resulting in an irreversible inactivation of some of the spiropyran cross-linkers linking with the damaged polymer chains.

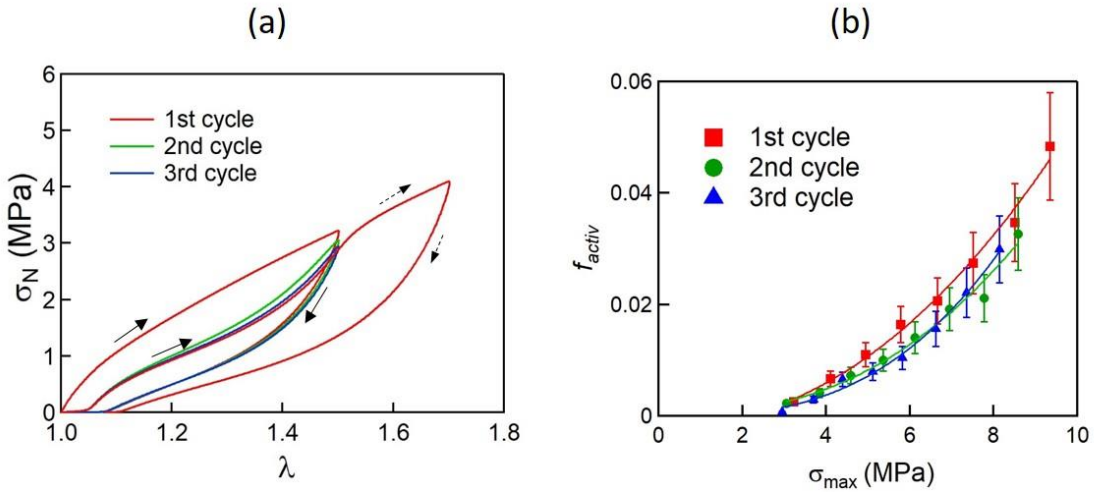

Figure 7 – Mullin's effect in the sample NP4VS1 at repeated 3 cycles of loading to the same maximum stretch values: (a) the stress-strain curves; (b) the mechanophore activation as a function of the maximum loading stress value.

Discussion

In this section, we propose possible mechanisms of nanocomposite deformation to explain our main experimental observations:

- The introduction of silica fillers in the cross-linked polyacrylate matrix leads to strong cavitation under stretch; this effect has been reported in the nanocomposite

literature[32,33], however, it was ignored in recent papers about mechano-activation in nanocomposites;

- The small-strain modulus of nanocomposites is mostly determined by the filler fraction and increases strongly with Φ_{SiO2}; this is characteristic for nanocomposites filled with fractal aggregates;
- At high strain, we observe mechanoactivation of spiropyran to merocyanine and the activation function $f_{activ}(\sigma_{max})$ is similar between nanocomposites with different volume fractions and interfacial coupling agents;
- The strain-softening observed in cyclic loading at the same level of nominal stress leads to a decrease in activation by rather modest 10-20%.

From different possible representations of the nanocomposite structure, we choose that with fractal-like filler aggregates dispersed in the elastomer matrix as schematically depicted on Figure 8. This structure is supported by our AFM and SEM observations and SAXS measurements. From these data, we may also estimate the silica nanoparticles average radius R_p = 15 nm. The aggregates of primary nanoparticles are polydisperse and irregularly shaped , and we may estimate their characteristic radius R_{agg} at about 50 nm. To predict the evolution of the structure of such a nanocomposite upon stretching, we need to compare the deformability of aggregate networks with respect to the matrix. We apply the criterion of Witten et al.[28] to find the characteristic radius for rigid aggregates:

$$R_{rigid} \sim R_p \left({E_{SiO2}}/{E_{rubber}} \right)^{1/(3+C)} \qquad (3)$$

At scales below R_{rigid}, the aggregate network may be considered as non-deformable with respect to the rest of the matrix. The connectivity parameter C characterizes the “tortuosity” of the aggregate network, i.e. how the shortest path length between two elementary particles

in a cluster scales with the Pythagorean distance between them. It is usually[34] comprised between 1 and 1.25. Taking C = 1, E_{SiO2} ≈ 10 GPa and E_{rubber} ≈ 1 MPa, we estimate R_{rigid} = 10 nm and R_p ~ 150 nm. This value is of the same order of value as the filler aggregate dimensions observed on the AFM images. Thus, we may represent the filler network as composed of rigid clusters of radius R_{rigid} containing the nanoparticle aggregates and the occluded rubber that is confined between two "arms" of a nanoparticle aggregate.

At small strains, the elastic modulus of such nanocomposite will be dominated by the effect of the filler network fraction and its percolation characteristics. Due to the low compliance of the aggregates, the matrix regions between them are over-stretched. The activation of mechanophores in the matrix regions confined between fillers occurs at lower overall stretch relative to the mechanophore in the bulk matrix, as shown by Kim at al[10]. The energy dissipation in this confined polymer may contribute to the nanocomposite reinforcement at small strains. However, the energy dissipation mechanisms in simple networks of poly(ethyl acrylate) at room temperature are weak[7] in comparison to tough nanocomposite matrices, which may show strain-induced crystallization, strong viscoelastic dissipation or sacrificial bond breaking,. The over-stretching in the confined regions between nanofiller aggregates will lead to cavitation and release the stress concentration when the local hydrostatic stress becomes sufficiently high to break the network. This explains the high level of whitening observed in the nanocomposites under load. At the same time, the mechanophore activation at small strains is negligible. We may speculate why the stress concentration and cavitation in the matrix regions confined between the aggregates network does not significantly activate spiropyran. Yet, the volume fraction of such confined regions may be quite low. Because of the damage of the polymer surrounding the cavity, the cavitation-related activation should be irreversible and might be partially responsible for the decrease of the activation in cyclic

loading as some of the network strands bearing spiropyran/merocyanine moieties will be broken and become permanently inactive. This may refine the arguments of Kim et al.[10] who observed an increased activation of spiropyran when it was confined between filler aggregates with respect to the case of homogeneous distribution in the matrix. Indeed, the fraction of the confined rubber in the nanocomposites studied in the present paper that are highly-stretched (and activate into MC) seems to be low. To support our hypothesis, we cite the data of Jouault et al.[35], who showed by combining Small Angle Neutron Scattering and SAXS that in polystyrene-silica nanocomposites of similar silica volume fraction above T_g, the matrix chains deformed in a similar manner as in the pure matrix.

At higher strains, the filler network is deformed and the aggregates are pulled away from each other in the tensile direction and pulled towards each other in the perpendicular directions. Because of the low compressibility of the aggregates with respect to the stretching compliance of the rubber, the deformation is non-affine. This leads to a local multi-layer structure with alternating layers of aggregate “rafts” and domains composed of mostly rubber matrix. A similar structure was suggested in the literature for different types of rubber nanocomposites based on SAXS measurements[16], in situ TEM imaging[20], AFM[36] and electrical conductivity measurements[21].

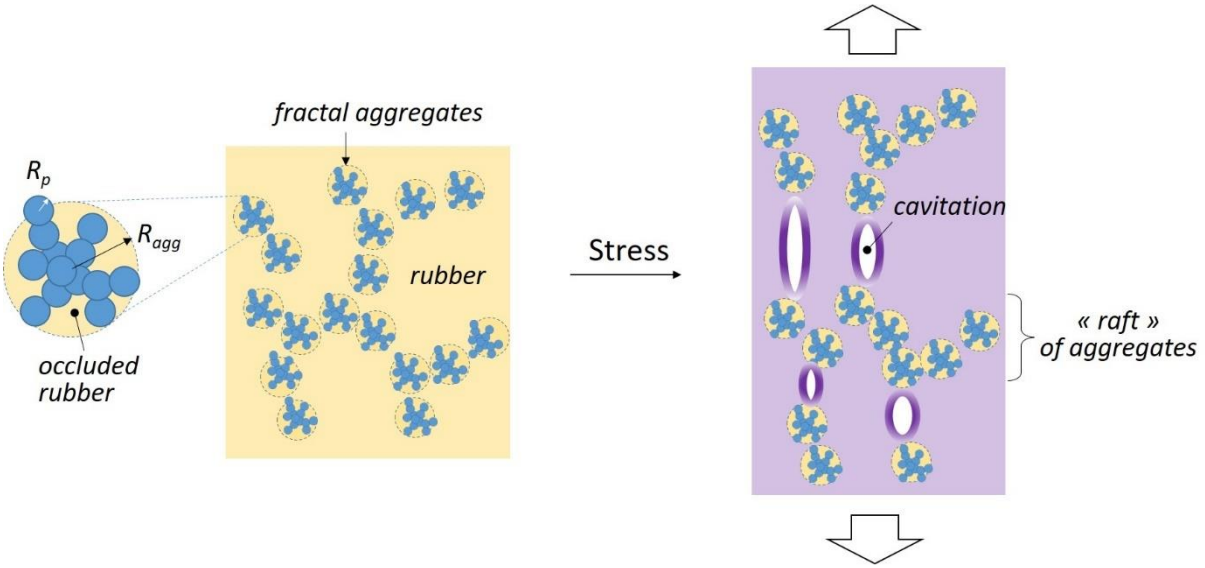

Figure 8 - The simple lattice scheme showing the nanocomposite deformation. The aggregates are considered as non-deformable at the scale R_{agg}.

The fact that a significant fraction of the spiropyran (about 1-10% of the total SP concentration) is activated in this large strain regime supports the idea that the rubber domains located between the "rafts" of the nanoparticle aggregates are highly stretched in the tensile direction. We have shown previously[3] that the concentration of activated spiropyran crosslinker embedded in the filler network of poly(ethyl acrylate) multiple networks follows a quadratic dependence on nominal stress with an activation threshold of about 2 MPa. In this proposed layered structure, the rubber bears a similar loading stress as the whole sample as it is loaded in series with the harder layers/rafts containing the aggregates. The tensile loading of the soft domains explains that a similar activation curve $f_{activ}(\sigma_{max})$ is observed for all nanocomposites. By contrast, the compression of aggregate "rafts" in the direction perpendicular to the tensile direction does not appear to lead to significant activation. While the compression of fractal aggregates was pointed out as an important mechanism[28] responsible for reinforcement, our results suggest that highly stretched chains in the matrix are dominant in our case. This is in line with results of Miyata et al.[20] who recently studied by transmission electron microscopy

the local strain distribution in a silica nanoparticle-filled isoprene rubber nanocomposites and showed that the higher strain localization in the overstretched domains is dominant with respect to the compressed areas inside aggregate “rafts”.

The limitations of our model to explain the activation master curve may be seen in Figure 9. Here, we show the differential tensile modulus $E_\lambda = d\sigma_N/d\lambda$ as a function of the stress. Unfortunately, due to the fragile nature of the matrix, we were not able to obtain its tensile curve at stretch values higher than 2.5. For all the samples, the moduli first decrease (the Payne effect), and next increase due to the finite chain extensibility in the elastomer. We notice that in the high-stress part of the curves the differential modulus follows a similar master curve that is independent of the sample. This tendency is qualitatively similar to the activation curves shown in previous sections and supports the presence of soft domains loaded in series with the hard domains of aggregate “rafts”, similar to the classic models of Nielsen[37] or Mullins and Tobias[31]. However, the observed high-strain E_λ values are several times higher than the modulus of the matrix and may not be explained by the over-stretching of the matrix. In this calculation of $E_\lambda = d\sigma_N/d\lambda$, we use the macroscopic stretch, which includes the low stretch of the incompressible rafts. This also suggests that the volume fraction of the non-deformable phase may be larger than we think.

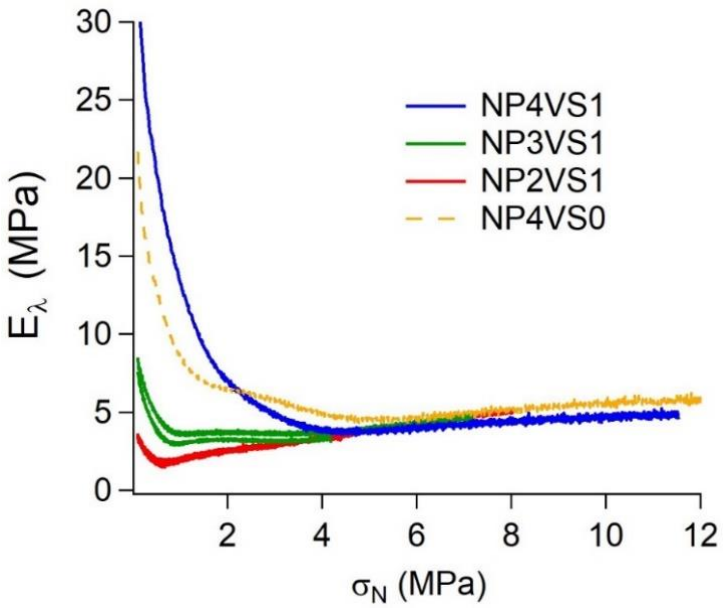

Figure 9 – Differential tensile modulus of nanocomposites depending on the nominal stress.

In the proposed mechanism, we neglected the effects of bond strength at the matrix/fillers interface. As shown in the literature[15], non-covalent coupling increases the possibility of interfacial slippage and detachment, leading to cavitation. The latter situation is most relevant for the sample NP4VS0 where only the non-covalent coupling agent is present at the matrix-filler interface. The effect of a weak interfacial coupling is indeed confirmed by a more pronounced plastic behavior and a stronger whitening of this sample relative to the VS1 series. The fact that the activation as a function of stress follows a very similar master curve as the one for the samples containing a covalent coupling agent supports the idea that the major part of activation is due to the stretching of the soft matrix domains.

Conclusion

We proposed a new protocol to synthesize under mild conditions (60°C), model poly(ethyl acrylate) elastomer nanocomposites filled with branched aggregates of silica nanoparticles

and labeled with spiropyran mechano-active cross-linkers. We observed that the nanocomposites change their color under tension, however, the detection and a quantitative determination of the concentration of activated molecules due to tensile stress is limited by a strong whitening of the samples due to cavitation that scatters the light. Nevertheless, we quantified the color change from analysis of the unloaded samples, due to the ability of the activated SP to remain in its activated state for several hours once the load is removed. We obtained the mechano-activation occurring after cycles of loading and unloading of the nanocomposites as a function of maximum stretch and maximum nominal stress during each cycle. We found that samples with different silica volume fractions and in presence or absence of covalent coupling between the filler and the matrix, have very similar levels of spiropyran activation at the same nominal maximum stress, although this corresponds to different values of stretch. Our finding strongly suggests that, for this class of nanocomposites, most of the load at high strain is carried by the polymer strands that are close to their maximum extensibility rather than by the transverse compression of silica aggregates. We also show that the Mullins softening of the nanocomposites leads to a slight decrease in level of activation during the second loading cycle. However, this decrease is low (about 10-20%) and the activation curves after 2^{nd} and 3^{rd} cycles follow the same evolution. We propose a mechanism of deformation of the aggregate network that may lead to a layered structure in which most of the rubber is loaded in series with the hard “rafts” of silica aggregates and is bearing the same load, which leads to similar activation curves. Thus, we may conclude that due to the reorganization and fragmentation of the filler network, the load is transferred from the hard aggregates to the soft polymer domains.

Supporting information

The supporting information file includes the TGA curves of the samples to determine the silica fractions, the details about fracture toughness determination and visible spectroscopy data normalization, complementary AFM and SEM images of nanocomposites, SAXS curves in additional representations and characterization of sample transparency under stretch.

Acknowledgments

This project has received funding from the *European Research Council (ERC) under the European Union's Horizon 2020 research and innovation program* under grant agreement AdG No 695351. We thank Mohamed Hanafi for his help with the TGA. We are grateful to Alba Marcellan, Joshua Yeh, Gabriel Sanoja, Rint Sijbesma, François Boué and Franck Vernerey for fruitful discussions.

References

(1) Chen, Y.; Mellot, G.; Luijk, D. van; Creton, C.; Sijbesma, R. P. Mechanochemical Tools for Polymer Materials. *Chem. Soc. Rev.* **2021**, *50* (6), 4100–4140. https://doi.org/10.1039/D0CS00940G.

(2) Caruso, M. M.; Davis, D. A.; Shen, Q.; Odom, S. A.; Sottos, N. R.; White, S. R.; Moore, J. S. Mechanically-Induced Chemical Changes in Polymeric Materials. *Chem. Rev.* **2009**, *109* (11), 5755–5798. https://doi.org/10.1021/cr9001353.

(3) Chen, Y.; Yeh, C. J.; Qi, Y.; Long, R.; Creton, C. From Force-Responsive Molecules to Quantifying and Mapping Stresses in Soft Materials. *Sci. Adv.* **2020**, *6* (20), eaaz5093. https://doi.org/10.1126/sciadv.aaz5093.

(4) Celestine, A.-D. N.; Sottos, N. R.; White, S. R. Strain and Stress Mapping by Mechanochemical Activation of Spiropyran in Poly(Methyl Methacrylate). *Strain* **2019**, *55* (3), e12310. https://doi.org/10.1111/str.12310.

(5) Früh, A. E.; Artoni, F.; Brighenti, R.; Dalcanale, E. Strain Field Self-Diagnostic Poly(Dimethylsiloxane) Elastomers. *Chem. Mater.* **2017**, *29* (17), 7450–7457. https://doi.org/10.1021/acs.chemmater.7b02438.

(6) Ducrot, E.; Chen, Y.; Bulters, M.; Sijbesma, R. P.; Creton, C. Toughening Elastomers with Sacrificial Bonds and Watching Them Break. *Science* **2014**, *344* (6180), 186–189. https://doi.org/10.1126/science.1248494.

(7) Slootman, J.; Waltz, V.; Yeh, C. J.; Baumann, C.; Göstl, R.; Comtet, J.; Creton, C. Quantifying Rate- and Temperature-Dependent Molecular Damage in Elastomer Fracture. *Phys. Rev. X* **2020**, *10* (4), 041045. https://doi.org/10.1103/PhysRevX.10.041045.

(8) Shannahan, L. S.; Lin, Y.; Berry, J. F.; Barbee, M. H.; Fermen-Coker, M.; Craig, S. L. Onset of Mechanochromic Response in the High Strain Rate Uniaxial Compression of Spiropyran Embedded Silicone Elastomers. *Macromol. Rapid Commun.* **2021**, *42* (1), 2000449. https://doi.org/10.1002/marc.202000449.

(9) Hong, G.; Zhang, H.; Lin, Y.; Chen, Y.; Xu, Y.; Weng, W.; Xia, H. Mechanoresponsive Healable Metallosupramolecular Polymers. *Macromolecules* **2013**, *46* (21), 8649–8656. https://doi.org/10.1021/ma4017532.

(10) Kim, T. A.; Lamuta, C.; Kim, H.; Leal, C.; Sottos, N. R. Interfacial Force-Focusing Effect in Mechanophore-Linked Nanocomposites. *Adv. Sci.* **2020**, *7* (7), 1903464. https://doi.org/10.1002/advs.201903464.

(11) Chen, Y.; Sanoja, G.; Creton, C. Mechanochemistry Unveils Stress Transfer during Sacrificial Bond Fracture of Tough Multiple Network Elastomers. *Chem. Sci.* **2021**, *12* (33), 11098–11108. https://doi.org/10.1039/D1SC03352B.

(12) Matsuda, T.; Kawakami, R.; Nakajima, T.; Gong, J. P. Crack Tip Field of a Double-Network Gel: Visualization of Covalent Bond Scission through Mechanoradical Polymerization. *Macromolecules* **2020**, *53* (20), 8787–8795. https://doi.org/10.1021/acs.macromol.0c01485.

(13) Diani, J.; Fayolle, B.; Gilormini, P. A Review on the Mullins Effect. *Eur. Polym. J.* **2009**, *45* (3), 601–612. https://doi.org/10.1016/j.eurpolymj.2008.11.017.

(14) Demassieux, Q.; Berghezan, D.; Cantournet, S.; Proudhon, H.; Creton, C. Temperature and Aging Dependence of Strain-Induced Crystallization and Cavitation in Highly Crosslinked and Filled Natural Rubber. *J. Polym. Sci. Part B Polym. Phys.* **2019**, *57* (12), 780–793. https://doi.org/10.1002/polb.24832.

(15) Ramier, J.; Chazeau, L.; Gauthier, C.; Stelandre, L.; Guy, L.; Peuvrel-Disdier, E. In Situ SALS and Volume Variation Measurements during Deformation of Treated Silica Filled SBR. *J. Mater. Sci.* **2007**, *42* (19), 8130–8138. https://doi.org/10.1007/s10853-007-1728-1.

(16) Zhang, H.; Scholz, A. K.; Vion-Loisel, F.; Merckel, Y.; Brieu, M.; Brown, H.; Roux, S.; Kramer, E. J.; Creton, C. Opening and Closing of Nanocavities under Cyclic Loading in a Soft

Nanocomposite Probed by Real-Time Small-Angle X-Ray Scattering. *Macromolecules* **2013**, *46* (3), 900–913. https://doi.org/10.1021/ma302325w.

(17) Pérez-Aparicio, R.; Vieyres, A.; Albouy, P.-A.; Sanséau, O.; Vanel, L.; Long, D. R.; Sotta, P. Reinforcement in Natural Rubber Elastomer Nanocomposites: Breakdown of Entropic Elasticity. *Macromolecules* **2013**, *46* (22), 8964–8972. https://doi.org/10.1021/ma401910c.

(18) Papon, A.; Montes, H.; Lequeux, F.; Guy, L. Nonlinear Rheology of Model Filled Elastomers. *J. Polym. Sci. Part B Polym. Phys.* **2010**, *48* (23), 2490–2496. https://doi.org/10.1002/polb.22151.

(19) Clough, J. M.; Creton, C.; Craig, S. L.; Sijbesma, R. P. Covalent Bond Scission in the Mullins Effect of a Filled Elastomer: Real-Time Visualization with Mechanoluminescence. *Adv. Funct. Mater.* **2016**, *26* (48), 9063–9074. https://doi.org/10.1002/adfm.201602490.

(20) Miyata, T.; Nagao, T.; Watanabe, D.; Kumagai, A.; Akutagawa, K.; Morita, H.; Jinnai, H. Nanoscale Stress Distribution in Silica-Nanoparticle-Filled Rubber as Observed by Transmission Electron Microscopy: Implications for Tire Application. *ACS Appl. Nano Mater.* **2021**, *4* (5), 4452–4461. https://doi.org/10.1021/acsanm.1c00009.

(21) Beutier, C.; David, L.; Sudre, G.; Cassagnau, P.; Heuillet, P.; Cantaloube, B.; Serghei, A. In-Situ Coupled Mechanical/Electrical Investigations of EPDM/CB Composite Materials: The Electrical Signature of the Mechanical Mullins Effect. *Compos. Sci. Technol.* **2022**, *218*, 109144. https://doi.org/10.1016/j.compscitech.2021.109144.

(22) Chen, Y.; Yeh, C. J.; Guo, Q.; Qi, Y.; Long, R.; Creton, C. Fast Reversible Isomerization of Merocyanine as a Tool to Quantify Stress History in Elastomers. *Chem. Sci.* **2021**, *12* (5), 1693–1701. https://doi.org/10.1039/D0SC06157C.

(23) Brûlet, A.; Lairez, D.; Lapp, A.; Cotton, J.-P. Improvement of Data Treatment in Small-Angle Neutron Scattering. *J. Appl. Crystallogr.* **2007**, *40* (1), 165–177. https://doi.org/10.1107/S0021889806051442.

(24) Genix, A.-C.; Baeza, G. P.; Oberdisse, J. Recent Advances in Structural and Dynamical Properties of Simplified Industrial Nanocomposites. *Eur. Polym. J.* **2016**, *85*, 605–619. https://doi.org/10.1016/j.eurpolymj.2016.08.028.

(25) Schaefer, D. w.; Rieker, T.; Agamalian, M.; Lin, J. s.; Fischer, D.; Sukumaran, S.; Chen, C.; Beaucage, G.; Herd, C.; Ivie, J. Multilevel Structure of Reinforcing Silica and Carbon. *J. Appl. Crystallogr.* **2000**, *33* (3–1), 587–591. https://doi.org/10.1107/S0021889800001199.

(26) Gherib, S.; Chazeau, L.; Pelletier, J. M.; Satha, H. Influence of the Filler Type on the Rupture Behavior of Filled Elastomers. *J. Appl. Polym. Sci.* **2010**, *118* (1), 435–445. https://doi.org/10.1002/app.31606.

(27) Mzabi, S.; Berghezan, D.; Roux, S.; Hild, F.; Creton, C. A Critical Local Energy Release Rate Criterion for Fatigue Fracture of Elastomers. *J. Polym. Sci. Part B Polym. Phys.* **2011**, *49* (21), 1518–1524. https://doi.org/10.1002/polb.22338.

(28) Witten, T. A.; Rubinstein, M.; Colby, R. H. Reinforcement of Rubber by Fractal Aggregates. *J. Phys. II* **1993**, *3* (3), 367–383. https://doi.org/10.1051/jp2:1993138.

(29) Kato, A.; Ikeda, Y.; Kasahara, Y.; Shimanuki, J.; Suda, T.; Hasegawa, T.; Sawabe, H.; Kohjiya, S. Optical Transparency and Silica Network Structure in Cross-Linked Natural Rubber as Revealed by Spectroscopic and Three-Dimensional Transmission Electron Microscopy Techniques. *JOSA B* **2008**, *25* (10), 1602–1615. https://doi.org/10.1364/JOSAB.25.001602.

(30) Hanson, D. E.; Hawley, M.; Houlton, R.; Chitanvis, K.; Rae, P.; Orler, E. B.; Wrobleski, D. A. Stress Softening Experiments in Silica-Filled Polydimethylsiloxane Provide Insight into a Mechanism for the Mullins Effect. *Polymer* **2005**, *46* (24), 10989–10995. https://doi.org/10.1016/j.polymer.2005.09.039.

(31) Mullins, L.; Tobin, N. R. Theoretical Model for the Elastic Behavior of Filler-Reinforced Vulcanized Rubbers. *Rubber Chem. Technol.* **1957**, *30* (2), 555–571. https://doi.org/10.5254/1.3542705.

(32) Ramier, J.; Chazeau, L.; Gauthier, C.; Stelandre, L.; Guy, L.; Peuvrel-Disdier, E. In Situ SALS and Volume Variation Measurements during Deformation of Treated Silica Filled SBR. *J. Mater. Sci.* **2007**, *42* (19), 8130–8138. https://doi.org/10.1007/s10853-007-1728-1.

(33) Zhang, H.; Scholz, A. K.; Vion-Loisel, F.; Merckel, Y.; Brieu, M.; Brown, H.; Roux, S.; Kramer, E. J.; Creton, C. Opening and Closing of Nanocavities under Cyclic Loading in a Soft Nanocomposite Probed by Real-Time Small-Angle X-Ray Scattering. *Macromolecules* **2013**, *46* (3), 900–913. https://doi.org/10.1021/ma302325w.

(34) Meakin, P.; Majid, I.; Havlin, S.; Stanley, H. E. Topological Properties of Diffusion Limited Aggregation and Cluster-Cluster Aggregation. *J. Phys. Math. Gen.* **1984**, *17* (18), L975–L981. https://doi.org/10.1088/0305-4470/17/18/008.

(35) Jouault, N.; Dalmas, F.; Said, S.; Di Cola, E.; Schweins, R.; Jestin, J.; Boué, F. Direct Small-Angle-Neutron-Scattering Observation of Stretched Chain Conformation in Nanocomposites: More Insight on Polymer Contributions in Mechanical Reinforcement. *Phys. Rev. E* **2010**, *82* (3), 031801. https://doi.org/10.1103/PhysRevE.82.031801.

(36) Le Diagon, Y.; Mallarino, S.; Fretigny, C. Particle Structuring under the Effect of an Uniaxial Deformation in Soft/Hard Nanocomposites. *Eur. Phys. J. E* **2007**, *22* (1), 77–83. https://doi.org/10.1140/epje/e2007-00013-2.

(37) Nielsen, L. E. Simple Theory of Stress-Strain Properties of Filled Polymers. *J. Appl. Polym. Sci.* **1966**, *10* (1), 97–103. https://doi.org/10.1002/app.1966.070100107.